IOP Publishing Journal of Physics: Condensed Matter
J. Phys.: Condens. Matter **26** (2014) 266006 (8pp) doi:10.1088/0953-8984/26/26/266006

Thermal string excitations in artificial spin-ice square dipolar arrays

D Thonig[1,2], S Reißaus[2], I Mertig[1,2] and J Henk[2]

[1] Max-Planck-Institut für Mikrostrukturphysik, Weinberg 2, D-06120 Halle (Saale), Germany
[2] Institut für Physik, Martin-Luther-Universität Halle-Wittenberg, D-06120 Halle (Saale), Germany

E-mail: dthonig@mpi-halle.de

Received 5 March 2014, revised 21 April 2014
Accepted for publication 25 April 2014
Published 10 July 2014

Abstract
We report on a theoretical investigation of artificial spin-ice dipolar arrays using a nanoisland shape adopted from recent experiments (Farhan *et al* 2013 *Nature Phys.* **9** 375). The number of thermal magnetic string excitations in the square lattice is drastically increased by a vertical displacement of rows and columns. We find large increments especially for low temperatures and for string excitations with quasi-monopoles of charges ±4. By kinetic Monte Carlo simulations we address the thermal stability of such excitations, thereby providing time scales for their experimental observation.

Keywords: spin-ice dipolar arrays, magnetic monopoles, classical spin model, micromagnetic simulations

(Some figures may appear in colour only in the online journal)

1. Introduction

Frustrated magnetic systems have become a topic of particular interest in condensed matter physics [1–3]. The geometrical frustration arises from the specific geometry of the system rather than from disorder. It leads to 'exotic' low-temperature states, for example spin ice. In pyrochlore lattices—prominent compounds are dysprosium and holmium titanate—the spins arranged in corner-sharing tetrahedra mimic the hydrogen positions in water ice [4]. Experiments have found evidence for the existence of magnetic monopoles in these materials [5, 6], showing properties of hypothetical magnetic monopoles postulated to exist in vacuum [7]. Nano-scale arrays of ferromagnetic single-domain islands can show an artificial spin ice as well [8, 9].

Artificial spin ice consists of twodimensional periodic arrangements of nanometer-sized magnets. These nanoislands are typically elongated to show a single-domain state [10, 11], modeled for example as a magnetic dipole; the magnetic moment of a single island then points in one of two directions. Because the nanoislands are isolated from each other, e.g. separated by a distance of the order of several hundred nanometer, they are coupled by the long-range dipole–dipole interaction [12, 13].

Typical geometries of the nano-scale arrays are honeycomb or square lattices, fabricated using microstructuring techniques which allow for fine-tuning to obtain specific properties [14]. Shifting the rows and columns of a square lattice vertically (figure 1) by an amount determined by the lattice spacing and the islands' dimensions, one can produce the same degree of degeneracy in the ground state as in pyrochlore spin ice [15, 16] and the same residual entropy as water ice at zero temperature [17].

An advantage of dipolar arrays is that their properties can be tuned by their dimensions and shape. However, being twodimensional, they capture properties of genuine threedimensional spin ice in rough outlines. By stacking planar nanoarrays, a three-dimensional artificial spin ice has been realized which exhibits excitations as in real spin ice systems [18].

Because of the specific geometries used so far, artificial spin ice was hardly thermally active [19]: for permalloy nanomagnets the magnetic moment of each island is in the order of some 10^7 Bohr magneton, equivalent to an interaction energy of about 10^{-19} J. Thus in simulations the activation temperature is much larger than the melting temperature of permalloy (1450 K). However in recent investigations by Farhan and coworkers thermal activation at $T = 420$ K has been shown for up to three hexagons of nanomagnets [20] and for a square lattice [21]. The theoretical investigation presented in this paper relies on the experimentally feasible nanoisland dimensions of [20] in order to study thermal excitations at room

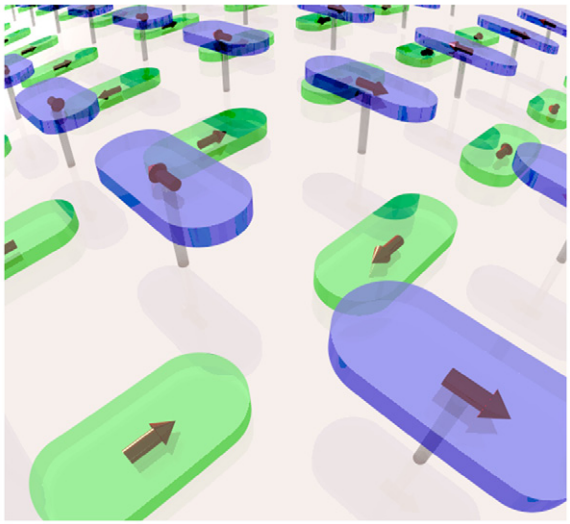

Figure 1. Artist's rendering of artificial spin ice on a square lattice of nanomagnets with vertically displaced rows and columns. Arrows indicate the direction of the magnetic moments.

temperature for square spin ice lattices. As one result we confirm the thermal activation at $T = 420$ K and below (e.g. at room temperature) found experimentally for the honeycomb lattice [20]. Moreover, the calculated switching rates of the nanomagnets are in the order of 0.2s^{-1}, thus accessible by experimental techniques.

In a ground state the square-lattice nanomagnets align according to the ice rule ('two in, two out') [16, 22]. Associating a magnetic charge Q to each node of the square lattice, a ground state is characterized by $Q = 0$ at each node. Excitations appear as reversals of dipoles, leading to nodes with a charge of ±2 or ±4. String excitations [22] are then given by a pair of these emergent quasi-monopoles [23, 24] with opposite charge that are connected by a ferromagnetic path of nanomagnets [21, 25]. While these strings have been produced experimentally by an external magnetic field, we focus in this paper on their thermal excitation. The response of the system to an external perturbation is observed by a variety of experimental techniques, for example photoemission electron microscopy [21, 26].

In the most part string excitations with $|Q| = 2$ nodes have been considered so far [16, 22, 27], which is attributed to the comparably small probability of $|Q| = 4$ string excitations. We show in this paper that the above-mentioned vertical displacement in the square lattice leads to a drastic increase of the number of $|Q| = 4$ string excitations, in particular at low temperatures. Moreover, we address the thermal stability of such excitations, thereby providing time scales for their experimental observation.

The paper is organized as follows. The theory is outlined in section 2, results are discussed in section 3. After addressing the magnetic ground state (section 3.1), we turn to the thermal string excitations: thermal activation and switching rates (section 3.2.1) as well as their number (section 3.2.2) and spatial correlation (section 3.2.3). Appendices comprise information on the dipolar energies (appendix A), the Monte Carlo simulations (appendix B) and the residual entropy (appendix C).

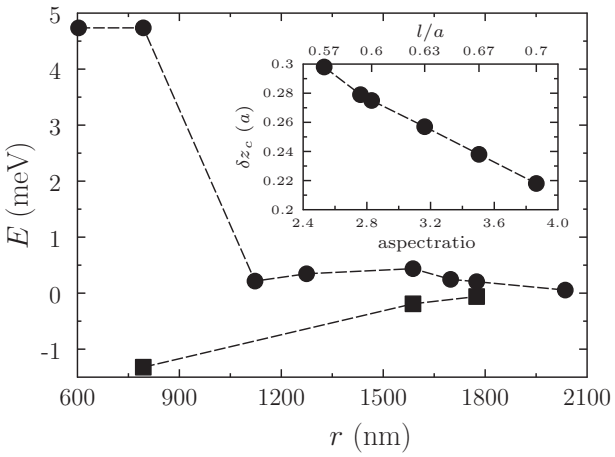

Figure 2. Dipolar energies E of nanomagnets on a square lattice versus distance r. The energy decreases (in absolute value) rapidly with distance r and can be neglected for distances larger than the second nearest neighbor distance ($r > 1000$nm). Some distances offer two energies, depending on the relative alignment of the nanoislands: nanoislands facing the long side (squares) offer a smaller energy than those facing the short side (circles). The inset shows the critical value δz_c for which the first and second nearest neighbor energies coincide versus the aspect ratio or the length l of the nanoislands (a, lattice constant). Lines are added to guide the eye.

2. Theoretical aspects

In this section we address those aspects of the theoretical approach needed for the discussion of the results. More details are given in the appendices.

For the present study we consider nanomagnets with dimensions taken from [20] (length 470nm, width 170nm, and height 3nm), since these exhibit thermal excitations at experimentally achievable temperatures. Each nanomagnet in the sample is labeled by an index i. The lattice constant a of the square lattice [8] is 793.8nm (the lattice spacing in [21] is 425nm). Due to their elongated shape and magnetic anisotropy they are in a single-domain state with magnetization parallel to the long edges of the islands. Their magnetic state is thus well described by a magnetization vector $\pm\vec{M}_i$. For permalloy islands of the above size one has $|\vec{M}_i| \approx 200 \cdot 10^3\,\text{A m}^{-1}$. Rows and columns are vertically displaced by δz which is given in units of a. Strictly speaking the twodimensional lattice is turned quasi-twodimensional for $\delta z \neq 0$ (figure 1).

Instead approximating the nanomagnets as points [15, 16, 22] or dipolar needles [15, 27], we compute the dipole–dipole energies for realistic shapes. The computation of the dipole–dipole energies is done numerically, allowing in principle for arbitrarily shaped nanoislands. It turns out that the dipolar interaction [13, 26] is relevant only for first-nearest neighbors and for second-nearest neighbors (figure 2), with energies $E_{1\text{NN}}$ and $E_{2\text{NN}}$, respectively [28].

The center $\vec{C}_i$ of a node i that consists of four nanomagnets at positions R_j (figure 3),

$$\vec{C}_i = \frac{1}{4}\sum_{j\in N_i}\vec{R}_j = \vec{R}_i + \frac{a}{2}(\vec{e}_x + \vec{e}_y)\,, \qquad (1)$$

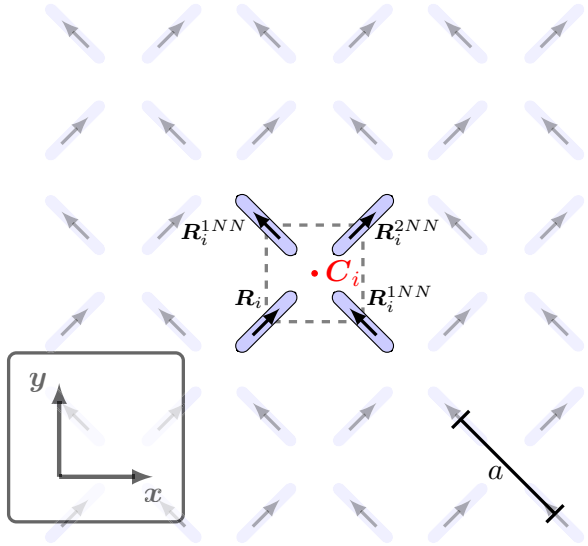

Figure 3. Square lattice of nanomagnets, forming a dipolar array. A node with center $\vec{C_i}$ is indicated by the dashed square and shows a '2in2outAd' configuration. Magnetic moments $\vec{M_i}$ of islands R_i and the two first nearest neighbors of R_i are represented as arrows and by R_i^{1NN}, R_i^{2NN}, respectively. The lattice parameter a is illustrated by the bold bar. The inset displays the Cartesian axes.

Table 1. Magnetic configurations of nodes, defined in [29]. Charges are defined in equation (2). The multiplicity gives the degree of degeneracy for each configuration. The energy of a node is expressed in terms of the first- and second-nearest neighbor energies E_{1NN} and E_{2NN}.

Configuration	Charge	Multiplicity	Energy
'4in'	+4	1	$4E_{1NN}+2E_{2NN}$
'3in1out'	+2	4	0
'2in2outAd'	0	4	$-2E_{2NN}$
'2in2outOp'	0	2	$-4E_{1NN}+2E_{2NN}$
'1in3out'	–2	4	0
'4out'	–4	1	$4E_{1NN}+2E_{2NN}$

carries a charge Q_i. This charge is defined by the number of magnetic dipoles pointing toward this node,

$$Q_i \equiv \sum_{j \in N_i} \frac{\vec{M_j} \cdot (\vec{C_i} - \vec{R_j})}{|\vec{M_j}||\vec{C_i} - \vec{R_j}|} \qquad (2)$$

leading to $Q_i \in \{0, \pm 2, \pm 4\}$.

The different magnetic configurations of the nodes are defined in table 1. The ice rule predicts groundstate configurations '2in2out' [29] which appear in two flavors: '2in2outAd' shows inward pointing moments at adjacent ('Ad') nanomagnets, whereas '2in2outOp' shows inward pointing moments at opposite ('Op') nanomagnets.

In accordance with the point group symmetry of the nodes the configurations are degenerate, as given by their multiplicity (table 1). For $\delta z = 0$, the least energy is produced by nodes with a '2in2outOp' arrangement ($-4E_{1NN}+2E_{2NN}$), with multiplicity 2 (see the four orange nanomagnets in figure 4; see [16]). The '2in2outAd' configuration (confer the four purple nanomagnets in figure 4) has an energy of $E = -2E_{2NN}$ and a multiplicity of 4.

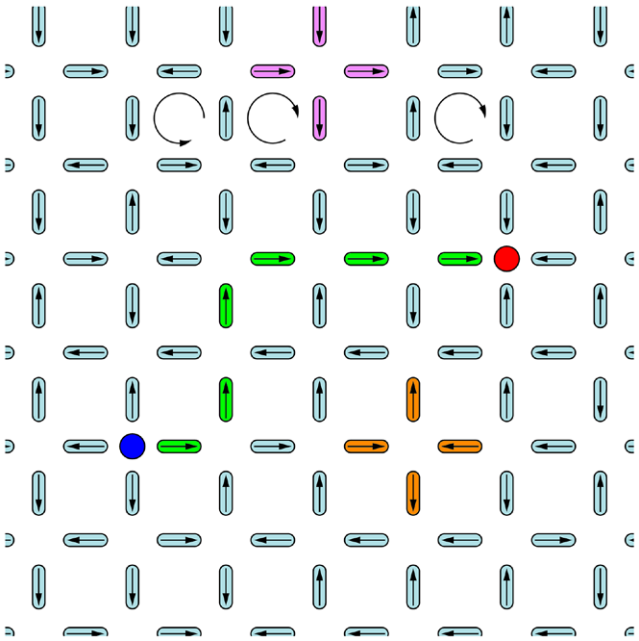

Figure 4. Snapshot of a magnetic configuration in square-lattice spin ice with $\delta z = 0.27\ a$ (a, lattice constant). A string excitation is formed by a quasi-monopole with charge $Q = -4$ (node with the blue circle) connected by a ferromagnetic string (path of six green nanomagnets) with a quasi-monopole with $Q = +4$ (node with the red circle). Arrows in each nanomagnet indicate the respective magnetization orientation. The four purple (orange) nanomagnets form a node with '2in2outAd' ('2in2outOp') configuration. For three plaquettes, the orientations of flux closures are shown by circular arrows. The snapshot, taken from a kinetic Monte Carlo simulation at $T = 300$ K, shows a part of the entire sample.

An increasing vertical displacement δz of rows and columns in the lattice results in a decrease of E_{1NN} (figure 5). E_{2NN} is unchanged because second-nearest neighbors are on the same or on adjacent rows or columns. At the special δz for which $E_{1NN} = E_{2NN}$ the degeneracy of the nodes' ground state is increased to 4 + 2 = 6 [16]. The honeycomb lattice possesses the same degree of degeneracy: the frustrated least-energy nodes with charges ±1 ('2in1out' or '2out1in') have a multiplicity of 3 each; showing identical energies, they are six-fold degenerate [23]. It is important to mention that in the honeycomb lattice this sixfold degeneracy is out of 8 possible vertices; in the square lattice considered here the sixfold degeneracy is out of 16 vertices (table 1). However, one may consider both lattices and their magnetic ground states equivalent because both have similar residual entropy (appendix C). Furthermore, the approach of E_{1NN} to E_{2NN} reduces the total energy and, thus, enhances the thermal activity, allowing simulations already for room temperature.

For the present samples, we obtain $\delta z = 0.27\ a$, which is a monotonous function of the lattice constant a (inset in figure 5). This value differs from those calculated for nanoscale arrays consisting of point or dipolar needles (0.419 a in [15], 0.444 a in [16] and 0.207 a in [15]). The limits given in the literature can be reproduced by varying the length l of the islands so that the volume and, thus, the magnetization density are conserved (inset in figure 2). We found a linear decrease

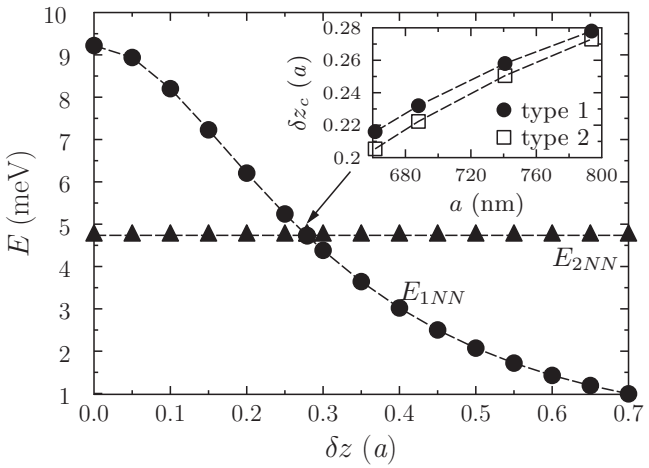

Figure 5. Dipolar energies of nanomagnets on a square lattice. Energies of first-nearest (1NN, filled circles) and second-nearest (2NN, filled triangles) nanoislands are shown versus the vertical displacement δz (in units of the lattice constant a). The arrow marks $\delta z = 0.27a$ for which $E_{1\mathrm{NN}} = E_{2\mathrm{NN}}$. The inset displays this critical point as a function of the lattice constant a. Filled circles and open squares indicate the crossing for rectangular (type 1) and rounded (type 2) islands, respectively. The dimensions of the nanomagnets and the lattice parameters are given in section 2.

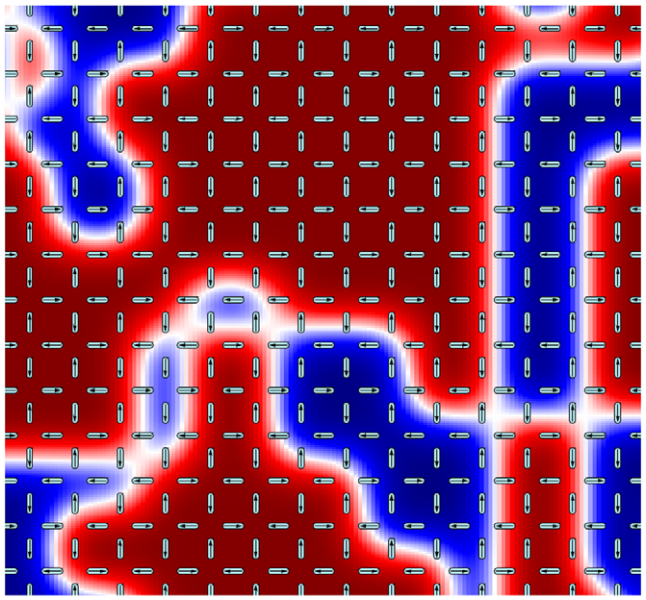

Figure 6. Magnetic ground state in square-lattice spin ice for a vertical displacement of $\delta z = 0.27\ a$ at $T = 0$ K. All six '2in2out' vertices are equally likely. The background color indicates '2in2outOp' (red) and '2in2outAd' (blue) domains.

of the critical point δz_c with respect to l/a. A linear regression yields $\delta z_c = 0.218a$ for $l = 0.7a$, a value close to the result of the dipolar needle approximation in [15]. δz_c in the point approximation [15, 16] is obtained for an aspect ratio of 1 for which the islands are squares; it reads $\delta z_c = 0.383a$. The minor differences are explained by a finite elongation of the islands and by the approximation of the short-range interaction: for a better comparison one could rely on $E_{1\mathrm{NN}} \equiv \sum_{i \neq 1\mathrm{NN}} E_i$ which is considered in [15] and [16].

The δz for which $E_{1\mathrm{NN}} = E_{2\mathrm{NN}}$ depends also moderately on the island shape (inset in figure 5). To check this we studied rectangular islands (type 1) with an aspect ratio of 2.76 (as in [20]) and rounded islands (type 2). The latter have the same area as type-1 islands but are composed of a rectangle with an aspect ratio of 1.98 and two terminating semi-circles with radii of 85nm. Because the shapes of type-1 and type-2 nanoislands are similar, the properties of the respective dipolar arrays are much the same as well, in particular their thermal excitations. Therefore, we restrict ourselves to presenting results for islands of type 2 in this paper; analyses of dipolar arrays of nanoislands with various shapes and dimensions will be performed in the future.

A string excitation is identified as a ferromagnetic path of nanoislands connecting a pair of nodes with opposite nonzero charges (figure 4). To quantify the thermal activation we address the fraction of nodes with charge Q in the sample, $\eta_Q \equiv N_Q/N$; on average $\langle \eta_Q \rangle = \langle \eta_{-Q} \rangle$.

In this paper we report on results for a lattice with 20 × 20 cells with 2 nanomagnets each ($N = 20 \times 20 \times 2 = 800$). These samples are large enough to suppress even minute finite-size effects (edge effects), as has been checked by comparison with calculations for larger arrays. The dynamics is obtained by kinetic Monte Carlo simulations, accompanied by standard Monte Carlo calculations [30, 31] (appendix B).

3. Discussion of results

In the following we focus on samples with vertical displacements δz of 0 and 0.27 a, as well as on temperatures $T \approx 1$ K and 300 K (room temperature).

3.1. Magnetic ground state

For a small finite temperature of $T \approx 1$ K we find a ground state in agreement with the ice rule (figure 6); hence, irrespectively of δz one has $\eta_0 = 100\%$. A closer inspection shows that '2in2outOp' vertices dominate for $\delta z = 0$, in agreement with earlier work (e.g. [16]). Upon increasing δz the number of '2in2outAd' vertices grows. Especially at $\delta z = 0.27\ a$ all six '2in2out' vertices are equally likely; this is explained by the energy barrier between the '2in2outAd' and ' 2in2outOp' vertices which vanishes for this particular vertical displacement.

The system tends to form '2in2outOp' and '2in2outAd' domains (figure 6) whose shapes depend on the numerical 'cooling-down' procedure used to obtain a global, highly degenerate free-energy minimum. For $\delta z > 0.27\ a$ '2in2outAd' vertices prevail. Elevated temperatures lead to changes of size and to propagation of domains.

3.2. Thermal string excitations

3.2.1. Thermal activation and switching rates. We now show that the square-lattice dipolar arrays are thermally active at room temperature and that the rate of spin reversals depends significantly on the vertical displacement δz. Thermal activity at 300 K cannot be ruled out *per se* because the maximum nearest-neighbor interaction energy $E_{1\mathrm{NN}}$ of 9.2meV is less than the thermal energy $k_B T \approx 25$meV (figure 5).

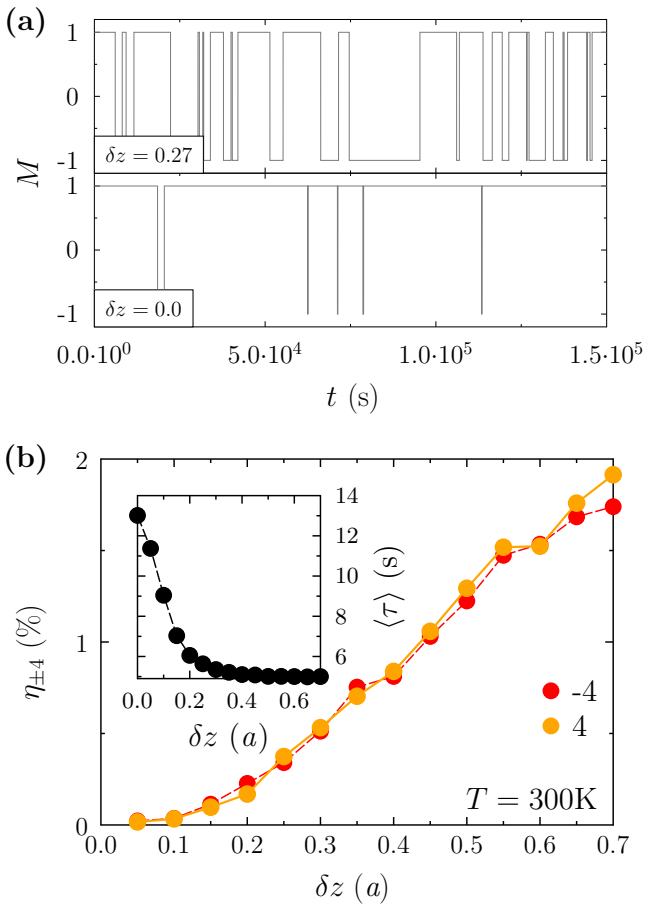

Figure 7. Thermal activation of square-lattice spin ice. (*a*) Representative time sequences of reversals of a selected nanomagnet, obtained from kinetic Monte Carlo simulations, are shown for vertical displacements $\delta z = 0.27a$ and 0.0 (indicated in each panel) at room temperature $T = 300$ K. $M = \pm 1$ characterizes the orientation of the selected magnetic moment. (*b*) Fractions of charges $\eta_{\pm 4}$ versus vertical displacement δz (a, lattice constant). The inset displays the average rest time $\langle \tau \rangle$ between consecutive reversals of the entire sample.

According to the implementation of the kinetic Monte Carlo method (appendix B and [32]), the rate τ^{-1} of spin reversals scales exponentially with temperature and the energy barrier since τ^{-1} follows an Arrhenius form. The barrier height depends on the initial and final configurational energies E_i and E_f and is assumed linear [33]: $\Delta E = E_0 + \frac{1}{2}(E_\mathrm{f} - E_\mathrm{i})$, where E_0 is an empirical parameter taken from [20].

Thermal activation is addressed by the duration—or rest time—between reversal of nanoislands. Figure 7(*a*) shows two representative sequences of magnetization reversal of one selected nanoisland; these could be measured by a local probe. Obviously the reversal rate is larger for $\delta z = 0.27\ a$ as compared to that for $\delta z = 0$; in other words, the rest time becomes smaller with increasing δz. For the sequences shown we obtain average rest times of $4.4 \cdot 10^3$s and $1.3 \cdot 10^4$s for $\delta z = 0.27\ a$ and 0, respectively, at $T = 300$ K.

Similar to the rest time of a single island, one can record the rest time of an entire sample. This duration is defined as the time between reversals of any nanoislands in the array. For arrays with 800 islands at $T = 300$ K, we obtain average rest times of 5.4s and 12.4s for $\delta z = 0.27\ a$ and 0, respectively. These values are smaller than that of a single island; they scale inversely with the number of islands in the sample. More precisely, they are about 1/800 of the single-island rest time. Because of the abovementioned Arrhenius behavior, rest times decrease significantly with temperature: for $T = 420$ K, as has been applied in [20], our simulations yield durations of the order of a few milliseconds.

We point out that the rest times should not be confused with the residence time defined in [20]. The residence time is defined as the duration between the reversal of the flux chirality of a plaquette (26 s for the hexagonal rings studied in [20]). Such a definition is somewhat problematic for a square lattice because its plaquettes must not show flux closure.

For zero vertical displacement $\delta z = 0$ the ground state '2in2outOp' nodes result in closed loops for the plaquettes; this can be viewed as energy-minimizing 'flux closures'. This is not the case for $\delta z = 0.27\ a$, for which there are '2in2outAd' nodes in addition (figure 4). This loss of flux closure is explained by the increased degeneracy of the '2in2out' nodes and a considerable number of nodes with charge $Q = \pm 2$ (top row in figure 4).

3.2.2. Number of string excitations. A finite temperature below the critical temperature of the nanoislands leads to thermal excitations with nonzero charge [34] (figure 8; note that $\langle \eta_Q \rangle = \langle \eta_{-Q} \rangle$): the larger $|Q|$, the smaller is $\langle \eta_{\pm Q} \rangle$. In particular, $\langle \eta_{\pm 4} \rangle$ is less than 2.3% for samples with $\delta z = 0$ at elevated temperatures; at room temperature it is extremely small.

A closer inspection reveals, however, that $\langle \eta_{\pm 4} \rangle$ is strongly enhanced for $\delta z = 0.\ 27\ a$ as compared to samples with $\delta z = 0$ (figure 8(*c*)). More precisely, there are about 3.5% quasi-monopoles with $|Q| = 4$ in the sample at 1200 K. Compared with the fraction of 2.3% for $\delta z = 0$ this increase may be regarded insignificant. However at room temperature, we find an enhancement by a factor as large as 43 (inset in figure 8(*c*)). Vertical displacement is therefore a means to enhance the number of excitations; their number may be sufficiently large to allow investigations of ensembles of string excitations [35].

So far we considered the fractions of nonzero charges in a sample. The presence of string excitations is evident from a snapshot of a kinetic Monte Carlo simulation (figure 4). While a large part of the sample shows a ground-state configuration, there is also a single string excitation: a path of ferromagnetically aligned nanomagnets (green nanomagnets in figure 4) connects a quasi-monopole of charge −4 (indicated by the blue circle, with '4out' arrangement) with a quasi-monopole of charge +4 (red circle, with '4in' arrangement).

3.2.3. Spatial correlation of string excitations. The spatial distribution of nodes with opposite charges is analyzed by means of the charge-correlation function

$$S_{\nu\mu}(|\delta\vec{r}|) \equiv \langle Q^{\nu}_{\vec{r}} Q^{\mu}_{\vec{r}+\delta\vec{r}} \rangle_{\vec{r}} \qquad (3)$$

which defines the probability of simultaneously finding a charge $Q = \mu$ at position $\vec{r} + \delta\vec{r}$ and a charge $Q = \nu$ at position $\vec{r}$. The average is over all nodes in the sample, thus $S_{\nu\mu} = S_{\mu\nu}$. It turns out that $S_{-4\,4}$ is nonzero within the first four shells of neighbor nanomagnets (circles in figure 9). According to the

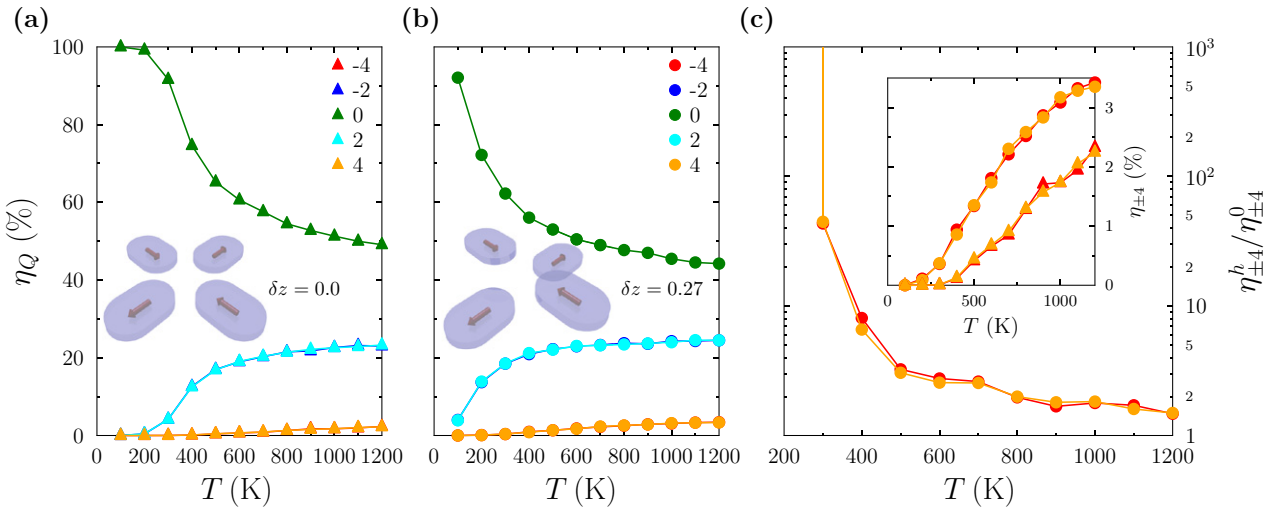

Figure 8. Magnetic charges Q in square-lattice dipolar arrays. The fractions η_Q of charges $Q = -4, \ldots, +4$ are shown for lattices with vertical displacement $\delta z = 0$ (*a*) and $\delta z = 0.27a$ (*b*) versus temperature T. Because $\eta_Q = \eta_{-Q}$ on average, data for negative charges are covered by those for positive Q. (*c*) Ratios $\eta_{\pm4}(0.27a)/\eta_{\pm4}(0)$ on a logarithmic scale versus temperature T. Monopole-charge fractions $\eta_{\pm4}$ for $\delta z = 0$ (triangles) and $\delta z = 0.27a$ (circles) (same data as in (*a*) and (*b*)) are given in the inset. Data are obtained by kinetic Monte Carlo simulations.

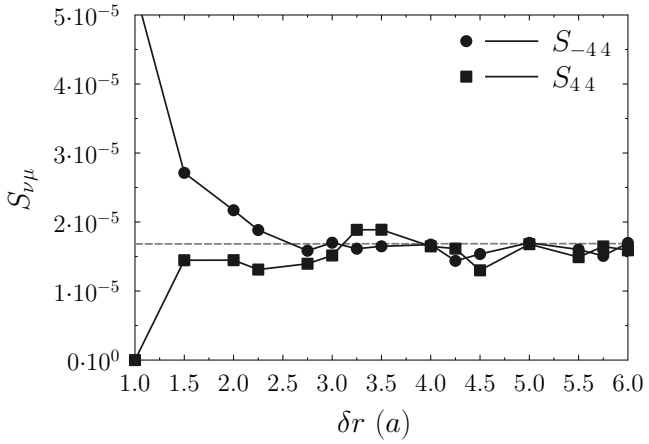

Figure 9. Charge-correlation function $S_{\nu\mu}$, equation (3), versus distance δr in square-lattice dipolar arrays at $T = 300$ K. Data are shown for S_{-44} (circles) as well as for S_{44} (squares). δr is in units of the lattice constant a. The dashed line indicates the saturation level for large distances.

free-energy minimization these pairs prefer to arrange with the shortest possible distance. Pairs of nodes with identical charges $Q = 4$ cannot show up as nearest neighbors because of the lattice geometry (one nanomagnet would be shared among a pair); hence, S_{44} equals zero for $\delta r = 0$. Furthermore, S_{44} is almost constant (squares in figure 9) which implies that pairs of $Q = 4$ nodes are not spatially correlated.

4. Concluding remarks

Square-lattice dipolar arrays prove suitable for studying thermal string excitations in artificial spin ice. By varying the vertical displacement of rows and columns, for example done by microstructuring techniques, one can produce samples with a prescribed temperature dependence of the string-excitation density. The thermal stability (mean average time) can be chosen to match the time resolution of the experimental probing technique.

Future investigations may focus on the effect of defects in the dipolar arrays (e.g. missing islands) or on the formation of domains.

Acknowledgments

This work is supported by the *Sonderforschungsbereich* 762 'Functionality of Oxide Interfaces'. DT is a member of the International Max Planck Research School on Science and Technology of Nanostructures, Halle, Germany. We thank Marin Alexe for fruitful discussions.

Appendix A. Interaction energies

The Heisenberg-type exchange is neglected in the calculations, owing to the fact that the nanomagnets are isolated from each other. Thus the dominant coupling mechanism comes from the dipole–dipole interaction. The total interaction energy then reads

$$E = -\sum_{i \neq j} \vec{m}_i \cdot \boldsymbol{Q} ij \cdot \vec{m}_j. \tag{A.1}$$

The magnetization density $\vec{m}_i = \dfrac{\vec{M}_i}{\Omega_i}$, where Ω_i is the volume of the i-th island, is assumed homogeneous.

Expressing a position $\vec{r}$ within the i-th nanomagnet by $\vec{r} \equiv \vec{R}_i + \vec{u}_i$, where $\vec{u}_i$ runs over its volume Ω_i, the elements of the dipole–dipole tensor $\boldsymbol{Q}_{ij}$ are

$$Q_{ij}^{\mu\nu} = \frac{\mu_0}{8\pi} \int_{\Omega_i} \int_{\Omega_j} \frac{3 r_{ij}^{\mu} r_{ij}^{\nu} - \delta_{\mu\nu} \vec{r}_{ij}^{\,2}}{\vec{r}_{ij}^{\,5}} d\vec{u}_j d\vec{u}_i, \tag{A.2}$$

with $\mu, \nu = x, y, z$. Here, $\vec{r}_{ij} \equiv \vec{u}_i + \vec{R}_i - \vec{u}_j - \vec{R}_j$ and μ_0 is the vacuum permeability.

Besides analytical calculations we use numerical integration schemes for the evaluation of the dipole–dipole tensor because these allow to treat arbitrarily shaped nanomagnets. For the present study, the integrals in (A.2) are performed using a Gauss–Legendre quadrature with 32 supporting points in each spatial direction. As a consequence of taking into account the experimental geometry of [20], the energy crossover $E_{1NN} = E_{2NN}$ (figure 5) occurs at a vertical displacement δz that is different from those calculated with a shape approximation for the nanomagnets; for example 0.419 a for needles [15] and 0.444 a for points [16].

It turns out that the first and the second nearest neighbors provide the relevant contributions to the interaction energy (figure 2); more precisely, $E_{3NN} = 0.045E_{1NN}$ and $E_{4NN} = 0.07E_{1NN}$ for δz = 0.27 a, with E_{1NN} being the first-nearest neighbor interaction energy. Interactions of second- and third-nearest neighbors do not depend on δz.

Lithographic techniques allow to produce nanomagnets with a specific shape. The chosen shape has evidently impact on the interaction energies although the lattice spacing may be unaltered. We briefly compare the interaction energies of two types with rectangular shape. Type 1 is strictly rectangular with an aspect ratio of 2.76 (as in [20]), type 2 is a rounded island with the same area as type 1, *i e* composed of a rectangle with an aspect ratio of 1.98 and circles with radius 85nm.

Having computed the set $\{Q_{ij}\}$ of dipole tensors we proceed with statistical methods that work on a discrete set in space (lattice of nanomagnets) and in the spin degrees of freedom (orientations of the nanomagnets' magnetizations).

Appendix B. Monte Carlo and kinetic Monte Carlo calculations

To simulate the ground state as well as the dynamics of the artificial spin ice Monte Carlo [36, 37] and kinetic Monte Carlo calculations have been performed. Both methods are implemented in the cahmd computer code [38, 39].

A Monte Carlo method tries to find a global minimum of the free energy at a given temperature T by successively reversing the island spins $\vec{M}_i$. Using the Metropolis algorithm [40] the reoriented state (final state) is accepted, if the energy difference $\Delta E = E_f - E_i$ between the initial and the final state is negative or if the Boltzmann factor $\exp(-\Delta E/k_B T)$ is larger than a uniformly distributed random number $p \in [0, 1]$. k_B is the Boltzmann constant.

In a kinetic Monte Carlo method the reorientation rate r_i for each spin $\vec{M}_i$ in the lattice follows an Arrhenius law,

$$r_i = \rho_0 \exp\left(\frac{-\Delta E_i}{k_B T}\right). \tag{B.1}$$

ΔE_i is the site-dependent energy barrier while ρ_0 is a fundamental rate fitted to experiment.

At each kinetic Monte Carlo step cumulative rates $\Gamma_i \equiv \sum_{j=1}^{i} r_j$ are calculated for i = 1, …, N (N number of nanomagnets). Then the magnetization of the i-th island is reversed if $\Gamma_{i-1} \leqslant p \cdot \Gamma_N < \Gamma_i$, with the random number p uniformly distributed in [0, 1] and $\Gamma_0 \equiv 0$. The rest time τ, *i e* the duration between two successive reversals in the entire sample, is $\tau = \Gamma_N^{-1} \ln(1/p')$ (p' uniformly-distributed random number).

The energy barrier ΔE_i in equation (B.1) is given by the dipolar energy and depends on the initial and the final state of the entire system. It is assumed linear [33]: $\Delta E_i \equiv E_0 + \frac{1}{2}(E_f - E_i)$. The larger E_0, the smaller are the rates and the larger are the rest times. ρ_0 and E_0 are empirical parameters and taken from [20] (E_0 = 0.925 eV, $\rho_0 = 10^{-12}$ s^{-1}). Both our standard and kinetic Monte Carlo approaches reproduce well the correlation functions and the switching rates for the hexagonal rings studied by Farhan *et al* [20].

The energy barrier depends on the dipole energy variation including the vertical displacement of the islands which increases the reorientation rate. In the picture of a Stoner–Wohlfarth double well potential, E_0 is determined by the magnetic anisotropy as well as by the inter-atomic magnetic exchange mechanisms [41].

For both standard and kinetic Monte Carlo simulations an initial 'cooling down', starting at $T = 5000$ K and approaching the chosen temperature of the simulation in 10 000 steps, has been performed to come close to a global free-energy minimum. A typical kinetic Monte Carlo simulation comprises at least 100 000 steps, with magnetic configurations saved to disk in intervals of 1000 steps. Average rest times $\langle\tau\rangle$ have been computed using all steps while average charge fractions $\langle\eta_Q\rangle$ are calculated from 100 samples.

Appendix C. Residual entropy

Following Pauling [17] a pyrochlore lattice contains $Z = (3/2)^{\frac{N}{2}}$ microstates for N spins, leading to the entropy per spin of $S = \frac{k_B}{N} \ln Z \approx 0.2 k_B$ (the factor of 2 comes from the two possible spin orientations). Considering a step-by-step build-up of a finite, vertically displaced spin-ice cluster from the top-left to the bottom-right corner, the ground state of a node with the center C_i is dominated by the configuration of its top and left node in the two adjacent islands. Depending on the relative alignment of the island spin coming from the top-node and the left-node, one obtains four possible states at node i. Neglecting rim effects the number of states ends up with $Z = (3/2)^{\frac{N}{2}}$ and the same residual entropy per spin for zero temperature as predicted by Pauling [17] for water ice. For $\delta z = 0$, however, the entropy per spin is $S = k_B\, 3/4\, ln\, 4/3$ [42], corroborating the preservation of the 'quasi-ice' character of the displaced system. Contrary to this the zero-point entropy of the honeycomb lattice is about $0.162 k_B$ [43], establish a slight difference of square and honeycomb dipolar arrays.

References

[1] Schiffer P 2002 Condensed-matter physics: magnetic frustration squeezed out *Nature* **420** 35–8

[2] Hodges J A, Dalmas P, Yaouanc A, Gubbens P C M, King P J C and Baines C 2011 Magnetic frustration in the disordered pyrochlore Yb_2GaSbO_7 *J. Phys.: Condens. Matter* **23** 164217

[3] Hamann J E *et al* 2012 Magnetic frustration, phase competition and the magnetoelectric effect in $NdFe_3\ (BO_3)_4$ *Phys. Rev. Lett.* **109** 267202

[4] Harris M, Bramwell S, McMorrow D, Zeiske T and Godfrey K 1997 Geometrical frustration in the ferromagnetic pyrochlore $Ho_2\ Ti_2\ O_7$ *Phys. Rev. Lett.* **79** 2554–7

[5] Bramwell S T and Gingras M J P 2001 Spin ice state in frustrated magnetic pyrochlore materials *Science* **294** 5546

[6] Gingras M J P 2009 Observing monopoles in a magnetic analog of ice *Science* **326** 375

[7] Dirac P A M 1931 Quantized singularities in the electromagnetic field *Proc. R. Soc. Lond.* A **133** 60–72

[8] Wang R F *et al* 2006 Artificial 'spin ice' in a geometrically frustrated lattice of nanoscale ferromagnetic islands *Nature Commun.* **439** 303–6

[9] Harris M J, Bramwell S T, McMorrow D F, Zeiske T and Godfrey K W 1997 Geometrical frustration in the ferromagnetic pyrochlore $Ho_2Ti_2O_7$ *Phys. Rev. Lett.* **79** 2554–7

[10] De'Bell K, MacIsaac B A, Booth N I and Whitehead P J 1997 Dipolar-induced planar anisotropy in ultrathin magnetic films *Phys. Rev.* B **55** 15108–18

[11] Stamps R and Camley R 1999 Magnetization processes and reorientation transition for small magnetic dots *Phys. Rev.* B **60** 11694–9

[12] Remhof A, Schumann A, Westphalen A, Zabel H, Mikuszeit N, Vedmedenko E, Last T and Kunze U 2008 Magnetostatic interactions on a square lattice *Phys. Rev.* B **77** 134409

[13] Mengotti E, Heyderman L J, Bisig A, Fraile A, Le Guyader L, Nolting F and Braun H B 2009 Dipolar energy states in clusters of perpendicular magnetic nanoislands *J. Appl. Phys.* **105** 113113–4

[14] Rougemaille N *et al* 2011 Artificial kagome arrays of nanomagnets: a frozen dipolar spin ice *Phys. Rev. Lett.* **106** 057209

[15] Möller G and Moessner R 2006 Artificial square ice and related dipolar nanoarrays *Phys. Rev. Lett.* **96** 237202

[16] Mól L A S, Moura W A and Pereira A R 2010 Conditions for free magnetic monopoles in nanoscale square arrays of dipolar spin ice *Phys. Rev.* B **82** 054434

[17] Pauling L 1935 The structure and entropy of ice and of other crystals with some randomness of atomic arrangement *J. Am. Chem. Soc.* **57** 2680

[18] Chern G-W, Reichhardt C and Nisoli C 2014 Realizing three-dimensional artificial spin ice by stacking planar nano-arrays *Appl. Phys. Lett.* **104** 013101

[19] Wysin G M, Moura W A, Mól L A and Pereira A R 2013 Dynamics and hysteresis in square lattice artificial spin ice *New J. Phys.* **15** 045029

[20] Farhan A, Derlet P M, Kleibert A, Balan A, Chopdekar R V, Wyss M, Anghinolfi L, Nolting F and Heyderman L J 2013 Exploring hyper-cubic energy landscapes in thermally active finite artificial spin-ice systems *Nature Phys.* **9** 375

[21] Farhan A, Derlet P M, Kleibert A, Balan A, Chopdekar R V, Wyss M, Perron J, Scholl A, Nolting F and Heyderman L J 2013 Direct observation of thermal relaxation in artificial spin ice *Phys. Rev. Lett.* **111** 057204

[22] Mól L A, Silva R L, Silva R C, Pereira A R, Moura W A and Costa B V 2009 Magnetic monopole and string excitations in two-dimensional spin ice *J. Appl. Phys.* **106** 063913

[23] Mengotti E, Heyderman L J, Fraile Rodríguez A, Nolting F, Hügli R V and Braun H-B 2010 Real-space observation of emergent magnetic monopoles and associated Dirac strings in artificial kagome spin ice *Nature Phys.* **7** 68–74

[24] Hügli R V, Duff G, O'Conchuir B, Mengotti E, Heyderman L J, Fraile Rodríguez A, Nolting F and Braun H B 2012 Emergent magnetic monopoles, disorder and avalanches in artificial kagome spin ice (invited) *J. Appl. Phys.* **111** 07E103 –5

[25] Pushp A, Phung T, Rettner C, Hughes B P, Yang S-H, Thomas L and Parkin S S P 2013 Domain wall trajectory determined by its fractional topological edge defects *Nature Phys.* **9** 505–11

[26] Mengotti E, Heyderman L, Fraile A, Bisig A, Le Guyader L, Nolting F and Braun H B 2008 Building blocks of an artificial kagome spin ice: photoemission electron microscopy of arrays of ferromagnetic islands *Phys. Rev.* B **78** 144402

[27] Möller G and Moessner R 2009 Magnetic multipole analysis of kagome and artificial spin-ice dipolar arrays *Phys. Rev.* B **80** 140409

[28] Vedmedenko E, Mikuszeit N, Oepen H and Wiesendanger R 2005 Multipolar ordering and magnetization reversal in two-dimensional nanomagnet arrays *Phys. Rev. Lett.* **95** 207202

[29] Morgan J P, Stein A, Langridge S and Marrows C H 2010 Thermal ground-state ordering and elementary excitations in artificial magnetic square ice *Nature Phys.* **7** 75–9

[30] Binder K 1979 *Monte Carlo Methods in Statistical Physics* (Berlin: Springer)

[31] Metropolis N 1987 The beginning of the Monte Carlo method *Los Alamos Science Special* (Los Alamos, NM: Los Alamos National Laboratory) p 125

[32] Kratzer P 2009 Monte Carlo and kinetic Monte Carlo methods ed J Grotendorst, N Attig, S Blügel and D Marx (Julich: Julich Supercomputing Centre) pp 51–76

[33] Fichthorn K A and Scheffler M 2000 Island nucleation in thin-film epitaxy: a first-principles investigation *Phys. Rev. Lett.* **84** 5371

[34] Kapaklis V *et al* 2012 Melting artificial spin ice *New J. Phys.* **14** 035009

[35] Gliga S, Kákay A, Hertel R and Heinonen O G 2013 Spectral analysis of topological defects in an artificial spin-ice lattice *Phys. Rev. Lett.* **110** 117205

[36] Binder K 1997 Applications of Monte Carlo methods to statistical physics *Rep. Prog. Phys.* **60** 487

[37] Böttcher D, Ernst A and Henk J 2012 Temperature-dependent Heisenberg exchange coupling constants from linking electronic-structure calculations and Monte Carlo simulations *J. Magn. Magn. Mater.* **324** 610

[38] CAHMD: Classical Atomistic Heisenberg Magnetization Dynamics 2013 A computer program package for atomistic magnetization dynamics simulations (Available from the authors electronic address: dthonig@mpi-halle.de)

[39] Böttcher D 2010 Theoretische Beschreibung der Magnetisierungsdynamik von Nanostrukturen *Master's Thesis* Martin-Luther-University Halle-Wittenberg

[40] Metropolis N, Rosenbluth A W, Rosenbluth M N and Teller E 1953 Equation of state calculations by fast computing machines *J. Chem. Phys.* **21** 1087

[41] Böttcher D, Ernst A and Henk J 2011 Atomistic magnetization dynamics in nanostructures based on first principles calculations: application to Co nanoislands on Cu(1 1 1) *J. Phys.: Condens. Matter* **23** 29

[42] Lieb E L 1967 Residual entropy of square ice *Phys. Rev.* **162** 162–72

[43] Moessner R and Sondhi S L 2003 Theory of the [1 1 1] magnetization plateau in spin ice *Phys. Rev.* B **68** 064411